



Published in final edited form as:

Nat Cell Biol. 2017 October ; 19(10): 1153–1163. doi:10.1038/ncb3607.

## Life-long hematopoiesis is established by hundreds of precursors throughout mammalian ontogeny

Miguel Ganuza<sup>1</sup>, Trent Hall<sup>1</sup>, David Finkelstein<sup>3</sup>, Ashley Chabot<sup>1</sup>, Guolian Kang<sup>2</sup>, and Shannon McKinney-Freeman<sup>§,1</sup>

<sup>1</sup>Department of Hematology, St. Jude Children's Research Hospital, Memphis, TN, 38105

<sup>2</sup>Department of Biostatistics, St. Jude Children's Research Hospital, Memphis, TN, 38105

<sup>3</sup>Department of Computational Biology, St. Jude Children's Research Hospital, Memphis, TN, 38105

### Summary

Current dogma asserts that mammalian life-long blood production is established by a small number of blood progenitors. However, this model is based on assays that require the disruption, transplantation and/or culture of embryonic tissues. Here, we used the sample-to-sample variance (SSV) of a multi-colored lineage trace reporter to assess the frequency of emerging life-long blood progenitors while avoiding the disruption, culture or transplantation of embryos. We find that approximately 719 Flk-1<sup>+</sup> mesodermal precursors, 633 VE-Cadherin<sup>+</sup> endothelial precursors and 545 *Vav1*<sup>+</sup> nascent blood stem and progenitor cells emerge to establish the hematopoietic system at embryonic days (E) 7-E8.5, E8.5-E11.5 and E11.5-E14.5, respectively. We also determined that the spatio-temporal recruitment of endothelial blood precursors begins at E8.5 and ends by E10.5 and that many c-Kit<sup>+</sup> clusters of newly specified blood progenitors in the aorta are polyclonal in origin. Our work illuminates the dynamics of the developing mammalian blood system during homeostasis.

### Introduction

Hematopoietic stem cells (HSCs) emerge during embryogenesis from mesodermally-derived *Runx1*<sup>+</sup> hemogenic endothelial cells (HE) in the dorsal aorta and arterial vasculature between embryonic day 10.5 (E10.5) and E11.5 of mouse ontogeny<sup>1</sup>. From here, they circulate to the fetal liver (FL), expand, and then seed the bone marrow (BM)<sup>1</sup>. Transplantation studies estimate <1 HSC/embryo at E10.5 and between 1-2 HSCs/embryo at

<sup>§</sup>Correspondence and request for materials should be addressed to S.M.-F. (Shannon.mckinney-freeman@stjude.org).

Supplementary Information is linked to the online version of the paper at [www.nature.com/nature](http://www.nature.com/nature).

**Author Contributions:** M.G. designed the study, analyzed *Confetti* mice, generated and performed iCC experiments, analyzed intra-aortic clusters, performed and analyzed transplants, collected and analyzed data, and wrote the paper. T.H. performed and analyzed transplants, contributed to study design, and analyzed data. D.F. performed computer simulations to derive the formula for estimating cell numbers, analyzed data, contributed to study design, and wrote relevant sections of paper. A.C. analyzed *Confetti*<sup>+</sup> blood and resulting data, G.K. performed statistical analyses, S.M.-F. designed the study, analyzed data, and wrote the paper. All authors discussed the results and commented on the manuscript.

**Author Information:** Reprints and permissions information is available at [www.nature.com/reprints](http://www.nature.com/reprints). The authors declare competing financial interests: details accompany the full-text HTML version of the paper at [www.nature.com/nature](http://www.nature.com/nature).

E11.5<sup>2-11</sup>. However, live imaging and multi-color fate mapping of zebrafish HE reveals much greater numbers of phenotypic HSCs and about 30 functional long-term HSC clones emerging from the mid-gestation dorsal aorta<sup>12-14</sup>. Recently, the reaggregation of mouse aorta-gonads-mesonephros (AGM) with BM-derived OP9 stromal cells and limiting dilution transplantation estimated 50 and 70 murine HSC precursors at E10.5 and E11.5, respectively<sup>15</sup>. It is impossible to know, however, if predictions made based on non-physiological *ex vivo* niches faithfully reflect *in vivo* HSC formation. Furthermore, recent work reveals that transplantation likely fails to read out the full repertoire of cells sustaining life-long hematopoiesis during homeostasis<sup>16-18</sup>. Thus, any transplantation-based approach almost certainly underestimates HSC and precursor numbers. Here, we sought to measure the number of independently specified precursors contributing to life-long hematopoiesis at distinct stages of mouse ontogeny using an approach unbiased by transplantation or *ex vivo* manipulation. We took advantage of the *ROSA26<sup>+</sup>/Confetti* allele (*Confetti* allele)<sup>19</sup>, which is recombined by *Cre recombinase* (CRE) to label cellular progeny randomly with GFP, YFP, RFP or CFP (*i.e.* *Confetti*-labeled cells) (Fig. 1a). Here, we establish that the SSV in the distribution of *Confetti*-colors in murine peripheral blood (PB) correlates with the number of cells initially labeled with CRE, either during embryogenesis or in adults. We exploit this observation to discover that hundreds of precursors emerge throughout mouse ontogeny to establish life-long hematopoiesis.

## Results

### SSV in the distribution of *Confetti*-colors predicts initiating cells in vitro

Classic studies successfully employed SSV, using the binomial or Poisson models, to estimate HSC numbers in adult mice<sup>20-24</sup>. Here, we took a similar approach to analyze the embryo using the *Confetti* allele<sup>19</sup> (Fig. 1a). This system has been used to visualize the clonal dynamics of solid tissue stem cells, but has not yet been applied to studies of hematopoiesis<sup>19,25</sup>. We hypothesized that the SSV in the distribution of *Confetti*-colors in the peripheral blood (PB) would correlate with the number of *Confetti*-labeled precursors contributing to life-long hematopoiesis such that large numbers of *Confetti*+ precursors would yield a low variance and a small number of *Confetti*+ precursors would produce a high variance (Fig. 1b). We tested this hypothesis empirically by generating an immortalized fibroblast cell line from *ROSA26<sup>ERT2-Cre/Confetti</sup>* mice (“inducible *Confetti* cells” or iCCs) (Fig. 1c). 4-OHT treatment of iCCs resulted in a distribution of *Confetti*-colors that was stable and specific to this cell line (Fig. 1d and Supplementary Fig. 1). Here, the GFP+ allele was under-favored, as has been previously reported<sup>19</sup>. We plated replicates of 5-50,000 4-OHT-treated iCCs, expanded these cells in culture, and then analyzed the distribution of *Confetti*-colors by flow cytometry (Fig. 1c). The coefficient of variance (CV, standard deviation/mean) amongst colors and between wells was calculated for each individual *Confetti*-color at each plated cell number. As expected, a decrease in the initial plated cell number correlated with an increase in the observed CV for each individual *Confetti*-color (Fig. 1e). From here onwards, CV will refer to the SSV in the distribution of the *Confetti*-colors. Next, we examined the average Log<sub>10</sub>(CV) for YFP, CFP and RFP versus the Log<sub>10</sub>(cell number) and observed a linear relationship between 50 and 2500 starting cells that yielded the following formula for estimating starting cell numbers based on SSV: cell

number =  $10^{(-1.56(\log_{10}CV) + 1.47)}$  (Fig. 1f, see Methods and Legend for additional details on formula derivation). This formula yielded accurate starting cell numbers estimates at *Confetti* labeling efficiencies of >3% and when >500 cells were analyzed (Fig. 1g-h, Supplementary Table 1).

### SSV in the distribution of *Confetti*-colors predicts the number of blood precursors in vivo

To assess if our formula could accurately estimate starting cell numbers when applied to hematopoiesis, CD45.1+CD45.2+ mice were transplanted with  $5 \times 10^6$ ,  $1 \times 10^6$  or  $2 \times 10^5$  whole bone marrow (WBM) cells isolated from CD45.2+ *ROSA26<sup>+</sup>/Confetti* *VE-Cadherin<sup>+</sup>/Cre* mice (Fig. 2a-b). Because blood derives from endothelium, *VE-cadherin<sup>+</sup>/Cre* labels the entire hematopoietic compartment<sup>26</sup>. Historically, the frequency of transplantable WBM HSCs is consistently estimated as about 1/10,000<sup>27-33</sup>. Thus, we expected recipients to engraft with about 500, 100 and 20 long-term HSCs (LT-HSCs), respectively. By 32 weeks post-transplant, in three independent experiments, the observed Log(CV) of the *Confetti*-colors in CD45.2+ PB estimated reconstitution with an average of  $592 \pm 260$ ,  $220 \pm 19$ , and  $121 \pm 16$  LT-HSCs in recipients of  $5 \times 10^6$ ,  $1 \times 10^6$  or  $2 \times 10^5$  WBM cells, respectively (Fig. 2b, Supplementary Table 2). As 20 initiating events falls outside our window of precision (Fig. 1f), it is not surprising that our formula did not accurately estimate this value. The Log(CV) of *Confetti*-colors in CD45.2+ PB at earlier time-points post-transplant (4-16 weeks) revealed large numbers of initiating events (*i.e.* repopulating units, RUs) in all transplanted mice (Fig. 2b). This number steadily declined over time in recipients. This pattern reflects the well established gradual exhaustion of short-term HSCs and progenitors over time post-transplant<sup>34-36</sup>. In a second experiment, *Confetti*+ WBM was transplanted at limiting dilution (Fig. 2a, 2c, Supplementary Fig. 2a-b). Here, the precise input of RUs could be independently confirmed by limiting dilution analysis (LDA). Our *Confetti*-based RU estimate correlated precisely with that predicted via LDA at 20 weeks post-transplant (Fig. 2c, Supplementary Fig. 2a-b, Supplementary Table 3). These experiments confirm that SSV in the distribution of *Confetti*-colors accurately reflects changes in initiating cell numbers in a reconstituting hematopoietic system.

Transplantable HSCs in the E11.5 AGM expand dramatically during *ex vivo* explant culture<sup>37</sup>. Thus, we tested if our *Confetti* approach could detect this increase. One to five embryo-equivalents (EE) of E11.5 AGM-derived cells were isolated from CD45.2+ *ROSA26<sup>+</sup>/Confetti* *VE-Cadherin<sup>+</sup>/Cre* embryos and transplanted into lethally irradiated CD45.1+CD45.2+ mice (Fig. 2d). There was significant CD45.2+ engraftment in 6/15 recipients (Fig. 2e). In two of these recipients, the CD45.2+ PB was primarily labeled with a single *Confetti* color (Fig. 2f), reflecting engraftment with very few HSCs. CD45.2+ PB in the remaining recipients was *Confetti*-, which is consistent with both a small number of engrafted HSCs and a recombination efficiency of only about 45% in *ROSA26<sup>+</sup>/Confetti* *VE-Cadherin<sup>+</sup>/Cre* mice (Supplementary Fig. 2c). This confirms previous reports that few newly specified HSCs are detected when transplanted into adult recipients<sup>2-4</sup>. E11.5 CD45.2+ *ROSA26<sup>+</sup>/Confetti* *VE-Cadherin<sup>+</sup>/Cre* AGMs were next cultured as explants for three days, dissociated, and then transplanted at 1EE into lethally irradiated CD45.1+CD45.2+ recipients (Fig. 2d). Here, 7/7 recipients displayed >90% CD45.2+ PB, of which 25-65% was *Confetti*+ (Fig. 2e-f). The resulting average Log<sub>10</sub>(CV) of the well-represented *Confetti*

colors of the CD45.2+ PB estimated that AGM-explant cell recipients were repopulated by 222 HSCs (95% CI[128,384]), Table 1, Supplementary Table 4, Supplementary Fig. 2d). These data confirm a >150-fold expansion of HSCs during *ex vivo* AGM explant culture, as reported previously<sup>37</sup>. The *de novo* appearance of *Confetti*<sup>+</sup> cells in the PB of AGM-explant recipients (Fig. 2f) indicates that some of this expansion is due to ongoing nascent specification, as previously reported<sup>37</sup>. This experiment further confirms that SSV in the distribution of *Confetti* colors faithfully reflects changes in initiating cell numbers *in vivo*.

We next tested our formula for estimating numbers of initiating cells in a non-transplant based biological context. Hematopoiesis in adult mice is sustained by thousands of hematopoietic progenitors<sup>16,18</sup>. Thus, we utilized tamoxifen (TAM) treated adult *ROSA26<sup>ERT2-Cre/Confetti</sup>* mice as a control for large numbers of PB contributing events, expecting low SSV of *Confetti*-colors to reflect large numbers of newly labeled independent clones (Fig. 3a-b). Four weeks after TAM-treatment, the *Confetti*<sup>+</sup> PB of *ROSA26<sup>ERT2-Cre/Confetti</sup>* mice was approximately 33% CFP, 33% RFP, 3% GFP and 29% YFP in all mature lineages examined (Supplementary Figs. 3a-c). As predicted, the observed SSV in the *Confetti*-colors was very low (Fig. 3c, Supplementary Table 4). This variance yielded an estimate of 8572 initiating events (95%CI[5943,12363]) (Table 1, Supplementary Table 4). This estimate agrees with recent reports of the highly polyclonal nature of hematopoiesis during homeostasis in adult mice<sup>16,18</sup>. To approximate small numbers of initiating events, we employed the *E2a* driver, which is first expressed by blastomeres during early murine development (Fig. 3a)<sup>38</sup>. *ROSA26<sup>+</sup>/Confetti<sup>+</sup>E2a<sup>+</sup>/Cre* mice thus represent a control for few initiating events and should yield a large SSV in PB *Confetti*-colors. Indeed, the observed variance in the PB of adult *ROSA26<sup>+</sup>/Confetti<sup>+</sup>E2a<sup>+</sup>/Cre* mice was very high and yielded an estimate of only 28 initiating events (95% CI[10, 81]) (Table 1, Fig. 3c, Supplementary Fig. 3a, Supplementary Table 4). Further, the distribution of *Confetti*-colors in the blood and other mesodermal, ectodermal, and endodermal tissues was similar and stochastic in individual *ROSA26<sup>+</sup>/Confetti<sup>+</sup>E2a<sup>+</sup>/Cre* mice, confirming *E2a*-Cre activation early in development in very few cells (Supplementary Figs. 3d-f). Thus, the estimated numbers of initiating events for both *ROSA26<sup>ERT2-Cre/Confetti</sup>* and *ROSA26<sup>+</sup>/Confetti<sup>+</sup>E2a<sup>+</sup>/Cre* mice demonstrate that our formula performs as expected in a biological context.

### Hundreds of embryonic precursors contribute to life-long hematopoiesis

We next sought to measure the number of independently specified precursors contributing to life-long hematopoiesis at distinct stages of mouse development. HSCs derive from hemogenic endothelium that is mesodermal in origin<sup>1</sup>. Thus, we interrogated the clonal complexity of hematopoietic precursors as they emerge from mesoderm and endothelium by analyzing the SSV of PB *Confetti*-colors in cohorts of *ROSA26<sup>+</sup>/Confetti<sup>+</sup>Fjk1<sup>+</sup>/Cre* (n=7) and *ROSA26<sup>+</sup>/Confetti<sup>+</sup>VE-Cadherin-Cre<sup>+</sup>/Cre* (n = 12) mice, which begin to express CRE in the mesoderm at E7 and the endothelium at E8.5, respectively<sup>26,39</sup>(Fig. 3a). We also examined cohorts of *ROSA26<sup>+</sup>/Confetti<sup>+</sup>Vav1<sup>+</sup>/Cre* (n=10) mice, which express CRE in newly specified hematopoietic stem and progenitor cells (HSPCs) beginning at E11.5 (Fig. 3a, Fig. 4a-b)<sup>40</sup>. *Confetti*-allele recombination efficiency ranged from 45% to 80% amongst these mouse strains (Supplementary Fig. 2c, Table 1). *Confetti* color distribution in the PB of

*ROSA26<sup>+</sup>/Confetti<sup>+</sup>Flk1<sup>+</sup>/Cre*, *ROSA26<sup>+</sup>/Confetti<sup>+</sup>VE-Cadherin<sup>+</sup>/Cre*, and *ROSA26<sup>+</sup>/Confetti<sup>+</sup>Vav1<sup>+</sup>/Cre* mice was similar to that observed in TAM-treated *ROSA26<sup>ERT2-Cre</sup>/Confetti<sup>+</sup>* mice (Supplementary Fig. 3a, c). By inputting the resulting average Log<sub>10</sub>(CV) of RFP, YFP, and CFP in the PB of each of these mouse cohorts into our formula for estimating cell numbers and adjusting for recombination efficiency, we calculated that approximately 719 (95% CI[713,726]), 633 (95% CI[524,763]) and 545 (95% CI[524,567]) mesodermal precursors, hemogenic endothelial precursors and newly specified HSPCs contribute to life-long hematopoiesis during mouse ontogeny, respectively (Fig. 3c, Table 1, Supplementary Table 4). These estimates were stable for 16 weeks of age for all mice (Supplementary Fig. 4d) and fell well within the cell range in which we empirically demonstrated that SSV in *Confetti*-colors is a reliable predictor of initiating cell numbers (Fig. 1f, Supplementary Table 1)<sup>2-4,15</sup>. We did not observe any dramatic differences in the number of precursors contributing to distinct blood lineages in these strains (Fig. 3f).

To validate these estimates using an unbiased system, *ROSA26<sup>+</sup>/Confetti<sup>+</sup>Ubiquitin<sup>+</sup>/ERT2-Cre* mice were subjected to a single dose of TAM at E7.5 (n=5) or E8.5 (n=6) (Fig. 3d). Here, CRE expression is ubiquitous and can be activated via TAM treatment<sup>41</sup>. The average Log<sub>10</sub>(CV) of RFP, YFP, and CFP in the PB of cohorts of *ROSA26<sup>+</sup>/Confetti<sup>+</sup>Ubiquitin<sup>+</sup>/ERT2-Cre* mice exposed to TAM at E7.5 and E8.5 yielded, respectively, estimates of 617 (95% CI[324,1174]) and 538 (95% CI[273,1057]) initiating events (Table 1, Supplementary Table 4). These data confirm that hundreds of precursors present between E7.5-E8.5 and E8.5-E9.5 contribute to life-long hematopoiesis.

*Vav1-Cre* drives CRE expression throughout FL hematopoietic ontogeny when FL HSPCs are thought to expand rapidly<sup>42-44</sup>. Given that *Vav1-Cre* labeling of hematopoietic cells begins at E11.5, we expected *Vav1-Cre* to capture this expansion and were therefore surprised that *Vav1-Cre* yielded similar initiating cell number estimates as *Flk1-Cre* and *VE-Cadherin-Cre* (Table 1, Supplementary Table 4). One technical explanation for this result is that *Vav1-Cre* driven labeling might saturate prior to the expansion of FL HSPCs. However, *Vav1-Cre* labeled 80% of adult PB but only about 33% of E13.5 and E14.5 CD45+c-Kit+ FL cells, suggesting that *Vav1-Cre* labeling has not yet saturated the hematopoietic system at these developmental time-points (Supplementary Figs. 2c, Figs. 4a-b). Further, we observed minimal delay in the onset of detectable *Confetti* fluorescence in 4-OHT-treated iCCs and recombination of the *Confetti* allele (Fig. 4c). However, we did note a slight delay between administration of 4-OHT and detectable DNA recombination (Fig. 4ci, Supplemental Fig. 6). Thus, altogether these data suggest the presence of a previously unappreciated developmental bottleneck in the FL, or temporally downstream of *Vav1-Cre*-dependent label saturation, that restricts the number of cells that ultimately establish the final pool of HSPCs that sustain life-long hematopoiesis. In sum, our data show that 600-700 precursors emerging first from the mesoderm and then from the endothelium before transiting through the FL ultimately establish the pool of HSPCs that sustain life-long hematopoiesis.



## Hemogenic endothelium is specified between E8.5-E10.5

We next sought to define the temporal window when HE precursors are specified. Here, we employed *ROSA26<sup>+</sup>/Confetti<sup>+</sup>Cdh5<sup>+</sup>/ERT2-Cre* mice, in which CRE activity is activated in the endothelium by TAM<sup>45</sup>. The temporal window post-delivery of TAM during which CRE is active has not been rigorously defined. To estimate this window, CD45.1+CD45.2+ mice treated with a single dose of TAM were transplanted with CD45.2+ *ROSA26<sup>ERT2-Cre</sup>/Confetti* WBM three, two, one or zero days after treatment (Fig. 5a). Here, *Confetti*+ PB was only detected in mice transplanted with *ROSA26<sup>ERT2-Cre</sup>/Confetti* WBM on the same day as TAM treatment (Fig. 5bi), despite high CD45.2+ PB engraftment in all recipients (>90%, Fig. 5bii). Recipients were treated with TAM 12 weeks post-transplant, resulting in 10-40% *Confetti*+ PB, confirming robust engraftment of *ROSA26<sup>ERT2-Cre</sup>/Confetti* WBM (Fig. 5biii and iv). These data suggest that the effective window of TAM-mediated *Confetti* allele recombination following a single treatment with TAM is <24 hours. Dams pregnant with *ROSA26<sup>+</sup>/Confetti<sup>+</sup>Cdh5<sup>+</sup>/ERT2-Cre* embryos were treated with a single dose of TAM at E7.5, E8.5, E9.5, E10.5 or E11.5 (Fig. 5c). Remarkably, 10-24 weeks after birth, *Confetti*+ cells were mostly observed in the PB of mice treated with TAM at E8.5 (~7% *Confetti*+ PB) and E9.5 (~8% *Confetti*+ PB) (Fig. 5d, Fig. 3f), with minimal labeling at E7.5. Labeling abruptly disappeared in the PB of mice treated with TAM at E10.5 and E11.5 (Fig. 5d), even though yolk sac and AGM endothelium were clearly labeled (Fig. 5e). Since the window of TAM activity is <24 hours, our data suggest that all HE throughout the embryo that contribute to life-long hematopoiesis are established by E10.25, after which new recruitment ceases. To test this further, E11.5 AGMs isolated from CD45.2+ *ROSA26<sup>+</sup>/Confetti<sup>+</sup>Cdh5<sup>+</sup>/ERT2-Cre* embryos subjected to TAM at E10.5 were cultured as explants for three days before transplantation into ablated CD45.2+CD45.1+ recipients (Fig. 5f). We and others have shown that nascent HSC specification occurs during AGM explant culture (Fig. 2e-f)<sup>37</sup>. Strikingly, *Confetti* labeling was undetectable in the CD45.2+ PB of 4/4 mice transplanted with AGM explant cells (Fig. 5g), confirming that recruitment of HE ceases before E10.5 and is not reactivated during AGM explant culture. The sum of the average estimate of the frequency of hemogenic precursors contributing to life-long hematopoiesis at E8.5 and E9.5 is ~660 (Table 1, Supplementary Table 4). Although the same hemogenic precursor might be *Confetti* labeled at both E8.5 and E9.5, this value matches our estimates of the number of hematopoietic precursors contributing to life-long hematopoiesis gleaned from *ROSA26<sup>+</sup>/Confetti<sup>+</sup>Fli1<sup>+</sup>/Cre*, *ROSA26<sup>+</sup>/Confetti<sup>+</sup>VE-Cadherin<sup>+</sup>/Cre*, and *ROSA26<sup>+</sup>/Confetti<sup>+</sup>Vav1<sup>+</sup>/Cre* mice.

## Many c-Kit+ intra-aortic clusters are polyclonal

Finally, we investigated the clonality of intra-aortic hematopoietic clusters (IACs) by examining the dorsal aorta of E11.5 *ROSA26<sup>+</sup>/Confetti<sup>+</sup>VE-Cadherin<sup>+</sup>/Cre* mice (Fig. 6a). Here, among c-Kit+ clusters harboring at least one *Confetti* color, 38/50 IACs 3 cells/cluster were a mixture of unlabeled cells and cells expressing distinct *Confetti*-colors (Fig. 6b, Supplementary Fig. 4 and 5a). These data suggest a polyclonal origin for many IACs. As polychromatic IACs could result from ongoing CRE activity, we examined CRE expression in VE-Cadherin+CD45- *Confetti*+ and *Confetti*- cells isolated from *ROSA26<sup>+</sup>/Confetti<sup>+</sup>VE-Cadherin<sup>+</sup>/Cre* E8.5 embryos, E9.5 caudal halves or E10.5 AGMs via qRT-PCR. We observed that CRE mRNA increased from E8.5 to E10.5 (Supplementary Fig. 5b). To functionally

examine the likelihood of ongoing CRE activity in *Confetti*<sup>+</sup> and *Confetti*<sup>-</sup> cells, VE-cadherin<sup>+</sup>CD45<sup>-</sup> *Confetti*<sup>-</sup>, CFP<sup>+</sup>, YFP<sup>+</sup>, or RFP<sup>+</sup> cells were isolated by flow cytometry from E10.5 *ROSA26*<sup>+/Confetti</sup> *VE-Cadherin*<sup>+/Cre</sup> embryos, cultured for seven days, and then analyzed for *Confetti*-labeling (Supplementary Fig. 5c and d). Cultured *Confetti*<sup>-</sup> cells remained *Confetti*<sup>-</sup> (Supplementary Fig. 5d). Expanded YFP<sup>+</sup>, CFP<sup>+</sup>, and RFP<sup>+</sup> cultures were composed nearly entirely of cells expressing the original *Confetti*-color plated (Supplementary Fig. 5d). These data suggest that color identity is fixed by E10.5 and are consistent with the idea that polyclonal clusters do not result from ongoing CRE activity post-specification. However, to definitively rule out this possibility, we examined c-Kit<sup>+</sup> IACs in E11.5 *ROSA26*<sup>+/Confetti</sup> *Cdh5*<sup>+/ERT2-Cre</sup> embryos treated with TAM at E7.5 and E8.5. Here, we also observed clusters composed of a mixture of unlabeled and *Confetti*<sup>+</sup> cells, further supporting that many IACs are polyclonal (Fig. 6a).

## Discussion

Recent studies have taken advantage of multicolor labeling to study unappreciated blood properties<sup>13,46</sup>. In zebrafish, a brainbow-based zebrafish system revealed that 30 HSC clones are present during peak production from aortic endothelium. Here, we analyze the clonal complexity of the emerging mammalian hematopoietic system using an approach that avoids transplantation, disruption or culture of the developing embryo. We observed that, within a defined range of initiating events (Fig. 1f), a linear relationship exists between the SSV in the distribution of *Confetti* allele-driven colors and the number of initially labeled cells. Via this approach, we estimated that between 600-700 developmental precursors contribute to life-long hematopoiesis. This is far greater than previous estimates of the frequency of HSC and HSPC precursors in the E10.5 and E11.5 AGM<sup>2-11,15</sup>. However, our data are consistent with the large number of IACs observed in E10.5 embryos (609±84 c-Kit<sup>+</sup> cells in the dorsal aorta and about 300 in the vitelline and umbilical arteries)<sup>47</sup>. Our findings also agree with the rapid expansion (*i.e.* 200-fold) of nascent HSPCs during AGM explant culture (Fig. 2f, Table 1)<sup>37</sup>. Importantly, AGM explant culture likely underestimates this potential, as explant culture conditions are almost certainly sub-optimal relative to the *in vivo* specification niche. Further, transplantation-based methods of estimation yield a snapshot view of the frequency of functional HSCs at a given point in time, while our approach captures the cumulative formation of nascent HSPCs that emerge and then exit the AGM. Perhaps more importantly, our approach did not require an artificial *ex vivo* niche or nascent HSCs to repopulate adult recipients. Indeed, newly specified E9.5 yolk sac and E10.5 AGM HSPCs are more readily functionally detected when transplanted into neonatal, rather than adult mice<sup>48-51</sup>. These studies strongly suggest that many nascent HSPCs have not yet acquired the ability to robustly engraft the adult BM microenvironment.

We also report that the specification of HE from endothelium occurs between E8.5 and E10.5 of murine development, after which it abruptly quenches and cannot be reactivated. Recent reports in zebrafish suggest the presence of an active cellular niche promoting the specification of nascent HSCs from the HE<sup>52</sup>. Our data suggest that a similar niche may also exist during mammalian development. It would be interesting to explore whether the abrupt quenching of HE specification results from an active mechanism of suppression or the passive loss of critical signals that cease or become distal as the embryo develops and grows.

Our study exposed several unexpected layers of active regulation of hematopoietic development. Importantly, our data suggest the presence of a developmental bottleneck in or downstream of the FL that restricts the number of cells contributing to life-long hematopoiesis. We speculate that this “bottleneck” could represent finite niche space capable of supporting the expanding FL HSPC pool or early BM. Further, the polyclonal nature of many IACs suggests that the cells that form these clusters may be highly migratory (*i.e.* IACs may result from the migration and coalescence of multiple nascent HSPC throughout the dorsal aorta or other sites of active hematopoietic specification). Interestingly, clusters composed of only two cells (and labeled with at least one *Confetti*-color) were nearly always monoclonal (25/27, Fig. 6b), suggesting that many nascent HSPCs divide shortly after specification from HE before incorporating into larger IACs. Although it was recently demonstrated that some cluster-derived cells are functional HSCs *in vivo*, more work is required to determine if each cell within a cluster contributes to life-long hematopoiesis<sup>53</sup>.

In sum, our data reveal unexpected layers of active regulation of hematopoietic development, including a developmental bottleneck in or downstream of the FL and an abrupt quenching in the recruitment of hemogenic endothelium. Remarkably, we reveal that life-long mammalian hematopoiesis is founded by hundreds of mesodermal and endothelial precursors during embryogenesis.

## Supplementary Material

Refer to Web version on PubMed Central for supplementary material.

## Acknowledgments

We thank W. Clements, P. Holmfeldt, F. Camargo, S. Patel, L. Grimes, B. Hadland, I. Bernstein and the McKinney-Freeman laboratory and Department of Hematology at St. Jude Children's Research Hospital (St. Jude) for critical discussions and reading of the manuscript; D. Ashmun, S. Schwemberger, and J. Laxton for FACS support; C. Davis-Goodrum, Krista Millican and C. Savage for help with injections and timed pregnancies; V. Frohlich and J. Peters for help with confocal imaging; *Cdh5<sup>+</sup>/ERT2-Cre* mice were a gift from the laboratory of Dr. Ralf Adams (Max Planck Institute for Molecular Biomedicine, Germany) by way of Dr. Ann Zovein (UCSF, CA USA). *Vav1-Cre<sup>+T</sup>* mice were a gift from the laboratory of Thomas Graf (Center for Genomic Regulation, Spain) by way of Dr. Nancy Speck (University of Pennsylvania, PA USA). *VE-Cadherin-Cre<sup>+T</sup>* mice were a gift from the laboratory of Dr. Guillermo Oliver (Northwestern University, IL USA). This work was supported by the American Society of Hematology (S.M.-F.), the Hartwell Foundation (S.M.-F.), the NIDDK (K01DK080846 and R01DK104028, S.M.-F.), the American Lebanese Syrian Associated Charities (ALSAC) (S.M.-F. and St. Jude Cell & Tissue Imaging Center), and the NCI (P30 CA021765-35, SJCRH Cell & Tissue Imaging Center). The St. Jude Cancer Center Core Cytogenetics laboratory is supported by the National Cancer Institute at the National Institute of Health, (P30 CA21765) and ALSAC.

## References

1. Medvinsky A, Rybtsov S, Taoudi S. Embryonic origin of the adult hematopoietic system: advances and questions. *Development*. 2011; 138:1017–1031. doi:138/6/1017[pii]10.1242/dev.040998. [PubMed: 21343360]
2. Kumaravelu P, et al. Quantitative developmental anatomy of definitive haematopoietic stem cells/long-term repopulating units (HSC/RUs): role of the aorta-gonad-mesonephros (AGM) region and the yolk sac in colonisation of the mouse embryonic liver. *Development*. 2002; 129:4891–4899. [PubMed: 12397098]
3. Medvinsky A, Dzierzak E. Definitive hematopoiesis is autonomously initiated by the AGM region. *Cell*. 1996; 86:897–906. doi:S0092-8674(00)80165-8 [pii]. [PubMed: 8808625]



4. Muller AM, Medvinsky A, Strouboulis J, Grosveld F, Dzierzak E. Development of hematopoietic stem cell activity in the mouse embryo. *Immunity*. 1994; 1:291–301. [PubMed: 7889417]
5. de Bruijn MF, Speck NA, Peeters MC, Dzierzak E. Definitive hematopoietic stem cells first develop within the major arterial regions of the mouse embryo. *EMBO J*. 2000; 19:2465–2474. DOI: 10.1093/emboj/19.11.2465 [PubMed: 10835345]
6. Gekas C, Dieterlen-Lievre F, Orkin SH, Mikkola HK. The placenta is a niche for hematopoietic stem cells. *Dev Cell*. 2005; 8:365–375. doi:S1534-5807(04)00468-X[pii] 10.1016/j.devcel.2004.12.016. [PubMed: 15737932]
7. Gordon-Keylock S, Sobiesiak M, Rybtsov S, Moore K, Medvinsky A. Mouse extraembryonic arterial vessels harbor precursors capable of maturing into definitive HSCs. *Blood*. 2013; 122:2338–2345. DOI: 10.1182/blood-2012-12-470971 [PubMed: 23863896]
8. Mikkola HK, Gekas C, Orkin SH, Dieterlen-Lievre F. Placenta as a site for hematopoietic stem cell development. *Exp Hematol*. 2005; 33:1048–1054. doi:S0301-472X(05)00293-6 [pii] 10.1016/j.exphem.2005.06.011. [PubMed: 16140153]
9. Ottersbach K, Dzierzak E. The murine placenta contains hematopoietic stem cells within the vascular labyrinth region. *Dev Cell*. 2005; 8:377–387. DOI: 10.1016/j.devcel.2005.02.001 [PubMed: 15737933]
10. Robin C, et al. Human placenta is a potent hematopoietic niche containing hematopoietic stem and progenitor cells throughout development. *Cell Stem Cell*. 2009; 5:385–395. DOI: 10.1016/j.stem.2009.08.020 [PubMed: 19796619]
11. Yoder MC, Hiatt K. Engraftment of embryonic hematopoietic cells in conditioned newborn recipients. *Blood*. 1997; 89:2176–2183. [PubMed: 9058742]
12. Bertrand JY, et al. Haematopoietic stem cells derive directly from aortic endothelium during development. *Nature*. 2010; 464:108–111. doi:nature08738 [pii] 10.1038/nature08738. [PubMed: 20154733]
13. Henninger J, et al. Clonal fate mapping quantifies the number of haematopoietic stem cells that arise during development. *Nat Cell Biol*. 2017; 19:17–27. DOI: 10.1038/ncb3444 [PubMed: 27870830]
14. Kissa K, Herbomel P. Blood stem cells emerge from aortic endothelium by a novel type of cell transition. *Nature*. 2010; 464:112–115. doi:nature08761 [pii] 10.1038/nature08761. [PubMed: 20154732]
15. Rybtsov S, Ivanovs A, Zhao S, Medvinsky A. Concealed expansion of immature precursors underpins acute burst of adult HSC activity in foetal liver. *Development*. 2016; 143:1284–1289. DOI: 10.1242/dev.131193 [PubMed: 27095492]
16. Busch K, et al. Fundamental properties of unperturbed haematopoiesis from stem cells in vivo. *Nature*. 2015
17. Schoedel KB, et al. The bulk of the hematopoietic stem cell population is dispensable for murine steady-state and stress hematopoiesis. *Blood*. 2016
18. Sun J, et al. Clonal dynamics of native haematopoiesis. *Nature*. 2014; 514:322–327. DOI: 10.1038/nature13824 [PubMed: 25296256]
19. Snippert HJ, et al. Intestinal crypt homeostasis results from neutral competition between symmetrically dividing *Lgr5* stem cells. *Cell*. 2010; 143:134–144. DOI: 10.1016/j.cell.2010.09.016 [PubMed: 20887898]
20. Harrison DE, Astle CM, Lerner C. Number and continuous proliferative pattern of transplanted primitive immunohematopoietic stem cells. *Proc Natl Acad Sci U S A*. 1988; 85:822–826. [PubMed: 2893377]
21. Abkowitz JL, Golinelli D, Harrison DE, Guttorp P. In vivo kinetics of murine hemopoietic stem cells. *Blood*. 2000; 96:3399–3405. [PubMed: 11071634]
22. Chen J, Astle CM, Harrison DE. Development and aging of primitive hematopoietic stem cells in BALB/cBy mice. *Exp Hematol*. 1999; 27:928–935. [PubMed: 10340409]
23. Harrison DE, Astle CM, Stone M. Numbers and functions of transplantable primitive immunohematopoietic stem cells. Effects of age. *J Immunol*. 1989; 142:3833–3840. [PubMed: 2565928]

24. Zhong RK, Astle CM, Harrison DE. Distinct developmental patterns of short-term and long-term functioning lymphoid and myeloid precursors defined by competitive limiting dilution analysis in vivo. *J Immunol.* 1996; 157:138–145. [PubMed: 8683107]
25. Rios AC, Fu NY, Lindeman GJ, Visvader JE. In situ identification of bipotent stem cells in the mammary gland. *Nature.* 2014; 506:322–327. DOI: 10.1038/nature12948 [PubMed: 24463516]
26. Chen MJ, Yokomizo T, Zeigler BM, Dzierzak E, Speck NA. Runx1 is required for the endothelial to haematopoietic cell transition but not thereafter. *Nature.* 2009; 457:887–891. doi:nature07619 [pii] 10.1038/nature07619. [PubMed: 19129762]
27. Boggs DR, Boggs SS, Saxe DF, Gress LA, Canfield DR. Hematopoietic stem cells with high proliferative potential. Assay of their concentration in marrow by the frequency and duration of cure of W/W<sup>v</sup> mice. *J Clin Invest.* 1982; 70:242–253. [PubMed: 6124553]
28. Cho RH, Sieburg HB, Muller-Sieburg CE. A new mechanism for the aging of hematopoietic stem cells: aging changes the clonal composition of the stem cell compartment but not individual stem cells. *Blood.* 2008; 111:5553–5561. DOI: 10.1182/blood-2007-11-123547 [PubMed: 18413859]
29. Szilvassy SJ, Humphries RK, Lansdorf PM, Eaves AC, Eaves CJ. Quantitative assay for totipotent reconstituting hematopoietic stem cells by a competitive repopulation strategy. *Proc Natl Acad Sci U S A.* 1990; 87:8736–8740. [PubMed: 2247442]
30. Kiel MJ, Yilmaz OH, Iwashita T, Terhorst C, Morrison SJ. SLAM family receptors distinguish hematopoietic stem and progenitor cells and reveal endothelial niches for stem cells. *Cell.* 2005; 121:1109–1121. doi:S0092-8674(05)00540-4 [pii] 10.1016/j.cell.2005.05.026. [PubMed: 15989959]
31. Sieburg HB, et al. The hematopoietic stem compartment consists of a limited number of discrete stem cell subsets. *Blood.* 2006; 107:2311–2316. DOI: 10.1182/blood-2005-07-2970 [PubMed: 16291588]
32. Sudo K, Ema H, Morita Y, Nakauchi H. Age-associated characteristics of murine hematopoietic stem cells. *J Exp Med.* 2000; 192:1273–1280. [PubMed: 11067876]
33. Trevisan M, Yan XQ, Iscove NN. Cycle initiation and colony formation in culture by murine marrow cells with long-term reconstituting potential in vivo. *Blood.* 1996; 88:4149–4158. [PubMed: 8943849]
34. Jordan CT, Lemischka IR. Clonal and systemic analysis of long-term hematopoiesis in the mouse. *Genes Dev.* 1990; 4:220–232. [PubMed: 1970972]
35. Purton LE, Scadden DT. Limiting factors in murine hematopoietic stem cell assays. *Cell Stem Cell.* 2007; 1:263–270. DOI: 10.1016/j.stem.2007.08.016 [PubMed: 18371361]
36. Yang L, et al. Identification of Lin(-)Sca1(+)*kit*(+)CD34(+)*Flt3*- short-term hematopoietic stem cells capable of rapidly reconstituting and rescuing myeloablated transplant recipients. *Blood.* 2005; 105:2717–2723. DOI: 10.1182/blood-2004-06-2159 [PubMed: 15572596]
37. Taoudi S, et al. Extensive hematopoietic stem cell generation in the AGM region via maturation of VE-cadherin+CD45+ pre-definitive HSCs. *Cell Stem Cell.* 2008; 3:99–108. doi:S1934-5909(08)00283-X [pii] 10.1016/j.stem.2008.06.004. [PubMed: 18593562]
38. Lakso M, et al. Efficient in vivo manipulation of mouse genomic sequences at the zygote stage. *Proc Natl Acad Sci U S A.* 1996; 93:5860–5865. [PubMed: 8650183]
39. Motoike T, Markham DW, Rossant J, Sato TN. Evidence for novel fate of *Flk1*+ progenitor: contribution to muscle lineage. *Genesis.* 2003; 35:153–159. DOI: 10.1002/gene.10175 [PubMed: 12640619]
40. Stadtfeld M, Graf T. Assessing the role of hematopoietic plasticity for endothelial and hepatocyte development by non-invasive lineage tracing. *Development.* 2005; 132:203–213. DOI: 10.1242/dev.01558 [PubMed: 15576407]
41. Ruzankina Y, et al. Deletion of the developmentally essential gene *ATR* in adult mice leads to age-related phenotypes and stem cell loss. *Cell Stem Cell.* 2007; 1:113–126. DOI: 10.1016/j.stem.2007.03.002 [PubMed: 18371340]
42. Bowie MB, et al. Hematopoietic stem cells proliferate until after birth and show a reversible phase-specific engraftment defect. *J Clin Invest.* 2006; 116:2808–2816. DOI: 10.1172/JCI28310 [PubMed: 17016561]

43. Fleming WH, et al. Functional heterogeneity is associated with the cell cycle status of murine hematopoietic stem cells. *J Cell Biol.* 1993; 122:897–902. [PubMed: 8349737]
44. Morrison SJ, Hemmati HD, Wandycz AM, Weissman IL. The purification and characterization of fetal liver hematopoietic stem cells. *Proc Natl Acad Sci U S A.* 1995; 92:10302–10306. [PubMed: 7479772]
45. Wang Y, et al. Ephrin-B2 controls VEGF-induced angiogenesis and lymphangiogenesis. *Nature.* 2010; 465:483–486. DOI: 10.1038/nature09002 [PubMed: 20445537]
46. Yu VW, et al. Epigenetic Memory Underlies Cell-Autonomous Heterogeneous Behavior of Hematopoietic Stem Cells. *Cell.* 2016; 167:1310–1322 e1317. DOI: 10.1016/j.cell.2016.10.045 [PubMed: 27863245]
47. Yokomizo T, Dzierzak E. Three-dimensional cartography of hematopoietic clusters in the vasculature of whole mouse embryos. *Development.* 2010; 137:3651–3661. DOI: 10.1242/dev.051094 [PubMed: 20876651]
48. Yoder MC, et al. Characterization of definitive lymphohematopoietic stem cells in the day 9 murine yolk sac. *Immunity.* 1997; 7:335–344. doi:S1074-7613(00)80355-6 [pii]. [PubMed: 9324354]
49. Yoder MC, Hiatt K, Mukherjee P. In vivo repopulating hematopoietic stem cells are present in the murine yolk sac at day 9.0 postcoitus. *Proc Natl Acad Sci U S A.* 1997; 94:6776–6780. [PubMed: 9192641]
50. Fraser ST, Ogawa M, Yu RT, Nishikawa S, Yoder MC. Definitive hematopoietic commitment within the embryonic vascular endothelial-cadherin(+) population. *Exp Hematol.* 2002; 30:1070–1078. doi:S0301472X02008871 [pii]. [PubMed: 12225799]
51. Arora N, et al. Effect of developmental stage of HSC and recipient on transplant outcomes. *Dev Cell.* 2014; 29:621–628. DOI: 10.1016/j.devcel.2014.04.013 [PubMed: 24914562]
52. Damm EW, Clements WK. Pdgf signalling guides neural crest contribution to the haematopoietic stem cell specification niche. *Nat Cell Biol.* 2017
53. Boisset JC, et al. Progressive maturation toward hematopoietic stem cells in the mouse embryo aorta. *Blood.* 2015; 125:465–469. DOI: 10.1182/blood-2014-07-588954 [PubMed: 25301706]

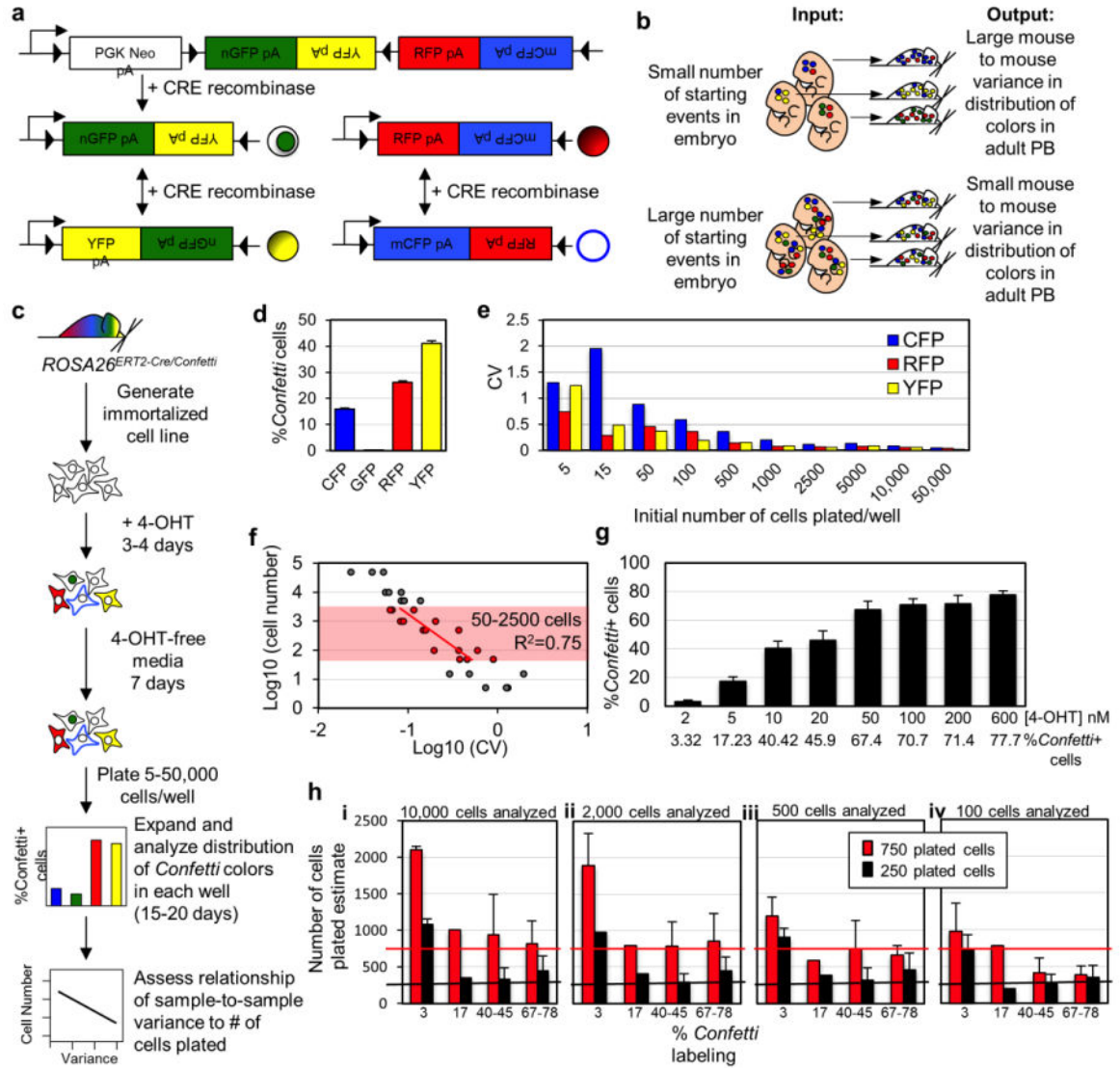


**Figure 1. Sample-to-sample variance reliably estimates number of initiating events**  
**a**, Schematic of *Confetti* allele. **b**, Sample-to-sample variance in the distribution of *Confetti* colors (output) inversely correlates with initiating events (input). **c**, Schematic of iCC experiment. **d**, *Confetti* labeling of 4-OHT treated iCCs. **e**, Well-to-well coefficient of variance (CV, standard deviation/mean) of each *Confetti* color in expanded iCCs. **f**, Average  $\text{Log}_{10}(\text{CV})$  of RFP, CFP, and YFP vs.  $\text{Log}_{10}(\text{cells plated/well})$ . Shaded region indicates cell range in which slope minimally diverged from slope of  $\text{Log}_{10}(\text{CV})$  vs.  $\text{Log}_{10}$  (starting cell number) line yielded in simulations (50-2500 cells, Supplemental Fig. 1c). Linear regression yielded:  $\text{cell number} = 10^{(-1.56 * \text{Log}_{10}(\text{CV}) + 1.47)}$  with 95% confidence intervals defined by cell number =  $10^{(-2.1 * \text{Log}_{10}(\text{CV}) + 1.06)}$  (lower bound) and cell number =  $10^{(-1.02 * (\text{Log}_{10}(\text{CV}) + 1.89)}$  (upper bound). This linear regression had an  $R^2$  of 0.75 and an adjusted  $R^2$  of 0.73 and p-value  $< 0.00001$  ( $F(1,13) = 39.21$ ). For the 15 residuals within the range tested the skew was 0.06 and the kurtosis 2.34, where a perfectly normal distribution would have a skew of 0 and a kurtosis of three. **d, e, f**, Results represent 3 independent similar experiments. **g**,

Labeling efficiency of iCCs treated with different concentrations of 4-OHT. Error bars indicate  $\pm$ s.d. of mean (n=9). This experiment was repeated twice. **h**, *Confetti*-based estimates were normalized to labeling efficiency as follows: Total initiating events = Estimate\*(100/% *Confetti*+ cells). The resulting reporter labeling efficiencies were grouped into four categories (3%, 17%, 40-45% and 67-78%). The average *Confetti*-based estimate of numbers of initially plated cells after normalization is shown (error bars indicate  $\pm$  s.d. of mean). *Confetti*-based estimates of numbers of initiating events maintains fidelity when the labeling efficiency is >3% and >500 cells are examined. Estimates were obtained from n 9 plated replicates. Results represent two independent similar experiments.

Author Manuscript

Author Manuscript

Author Manuscript

Author Manuscript



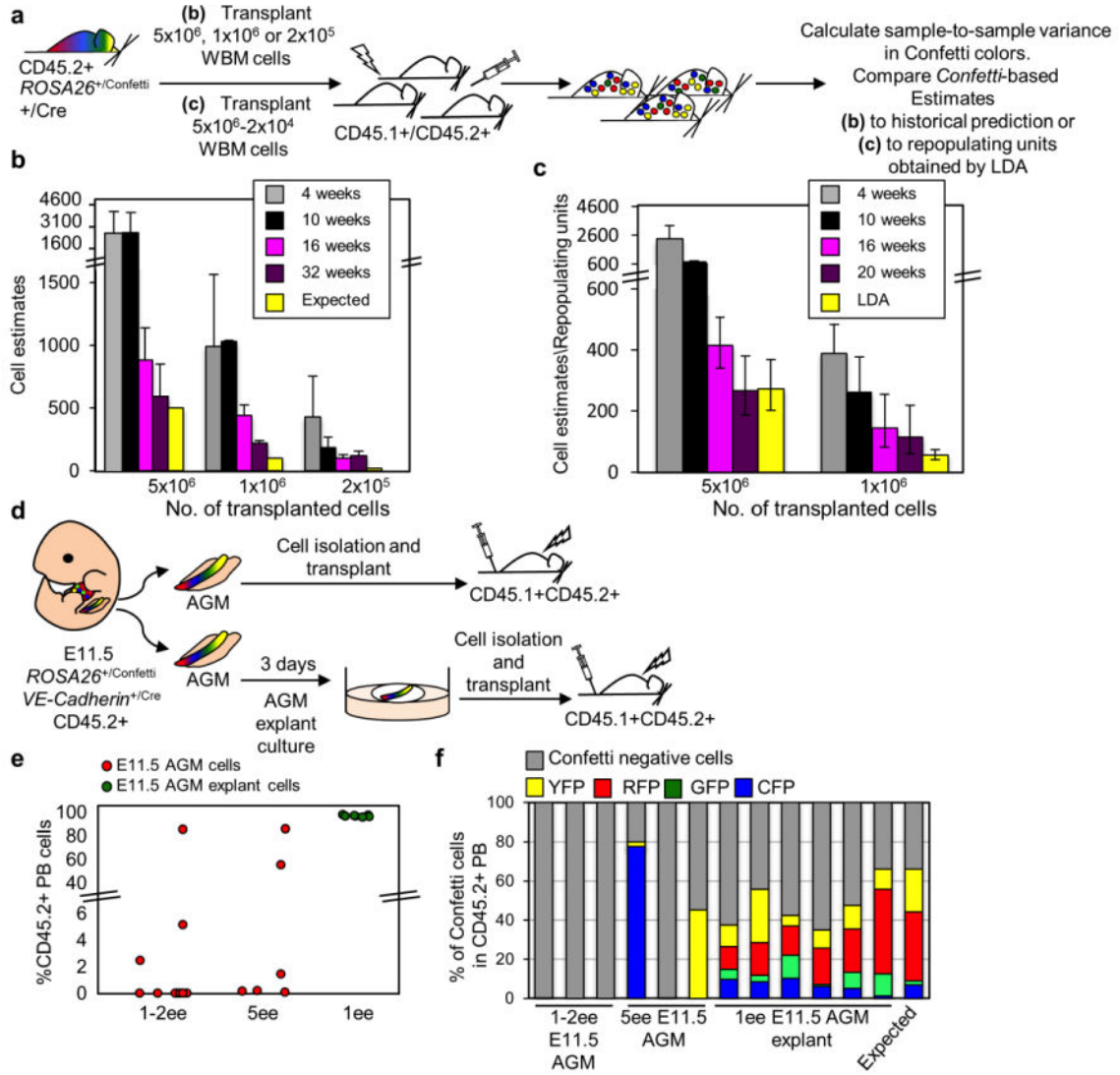


**Figure 2. Mouse-to-Mouse peripheral blood Confetti variance reliably estimates number of repopulating units after transplantation**

**a**, Experimental schematic. Here, “+/Cre” refers to any mouse heterozygous for CRE. **b**, 5x10<sup>6</sup>, 1x10<sup>6</sup>, 2x10<sup>5</sup>  $ROSA26^{+/Confetti} VE-Cadherin^{+/Cre}$  WBM cells were transplanted into irradiated mice. Sample-to-sample variance in the PB Confetti colors estimated the number of repopulating units (RUs). Confetti estimate of RU relative to expected number of RU based on historical controls (i.e. 1 LT-HSC/10,000 WBM cells). Data are the average of 3 independent experiments (Supplementary Table 2). Error bars = s.d. **c**, CD45.2+  $ROSA26^{+/Confetti} Flk1^{+/Cre}$  WBM was transplanted at limiting dilution into irradiated CD45.1+CD45.2+ mice along with 2x10<sup>5</sup> CD45.1+ WBM cells. Confetti colors in the CD45.2+ PB was examined between 4-20 weeks post-transplant, along with the distribution of total CD45.2+ PB chimerism (see Supplementary Fig. 2a-b). LDA indicates 1 RU/18,320 WBM cells transplanted (yellow bars, Supplementary Fig. 2b). Confetti-based estimates of RUs is shown at 4, 10, 16 and 20 weeks post-transplant. Error bars in LDA bar represent standard error. For Confetti-based estimates, error bars represent the 95% CI

(Supplementary Table 3). **d**, Experimental schematic. CD45.2+ *ROSA26*<sup>+/Confetti</sup> *VE-Cadherin*<sup>+/Cre</sup> cells from E11.5 AGM (n=16) or E11.5 AGM explants (n=7) were transplanted into irradiated CD45.1+CD45.2+ mice along with  $2 \times 10^5$  CD45.1+ WBM cells. **e**, %CD45.2+ PB 16 weeks post-transplantation. Each circle is an individual recipient. **f**, Frequency of unlabeled and *Confetti*<sup>+</sup> cells within CD45.2+ PB of recipients. Each bar is an individual recipient (Supplementary Table 4).

Author Manuscript

Author Manuscript

Author Manuscript

Author Manuscript

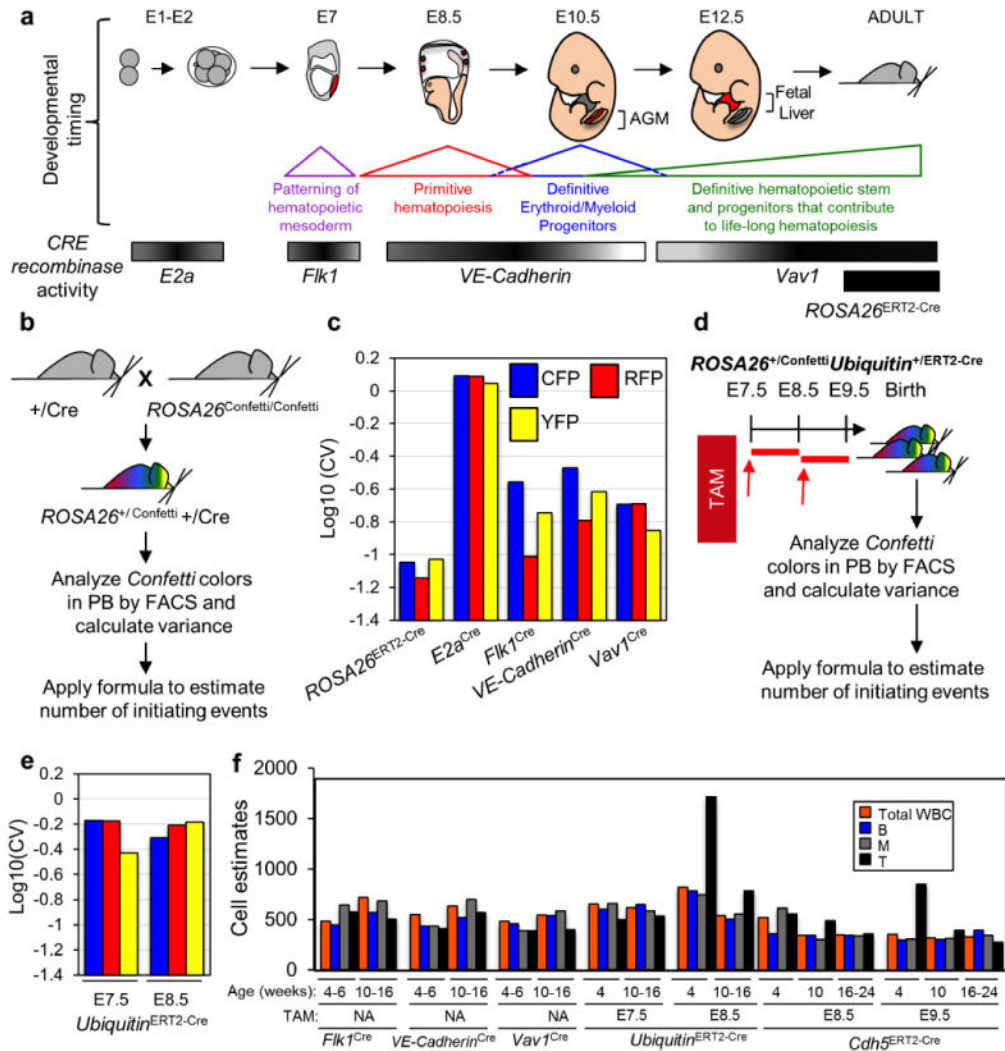


**Figure 3. Estimate of hematopoietic precursor numbers and activity during distinct stages of hematopoietic development**  
**a**, Schematic of window and site of CRE activity during murine development for  $E2a^{Cre}$ ,  $Flk1^{Cre}$ ,  $VE-Cadherin^{Cre}$  and  $Vav1^{Cre}$ .  $ROSA26^{ERT2-Cre}$  was activated by TAM in adult mice. **b**,  $+/Cre$  mice were mated with  $ROSA26^{Confetti/Confetti}$  and the resulting adult offspring analyzed by flow cytometry for *Confetti* labeling. **c**,  $\text{Log}_{10}(\text{CV})$  of each *Confetti* color in  $ROSA26^{+}/Confetti^{+}/Cre$  mice. GFP is excluded because it represented  $<10\%$  PB (Supplementary Table 4). **d**, 10 week old  $ROSA26^{+}/Confetti^{+} Ubiquitin^{+}/ERT2-Cre$  mice were analyzed for *Confetti* label after exposure to a single dose of TAM at E7.5 (n=5) or E8.5 (n=6). **e**,  $\text{Log}_{10}(\text{CV})$  of each *Confetti* color in  $ROSA26^{+}/Confetti^{+} Ubiquitin^{+}/ERT2-Cre$  mice. GFP is excluded because it represented  $<10\%$  PB (Supplementary Table 4). **f**, The number of precursors generating Myeloid (M), B-cells (B) and T-cells (T) are depicted in parallel to the global estimate (total white blood cells, WBC) in PB of adult (age indicated in weeks)  $ROSA26^{+}/Confetti^{+} Flk1^{+}/Cre$ ,  $ROSA26^{+}/Confetti^{+} VE-Cadherin^{+}/Cre$ , and  $ROSA26^{+}/Confetti^{+} Vav1^{+}/Cre$  mice.  $ROSA26^{+}/Confetti^{+} Ubiquitin^{+}/ERT2-Cre$  and

*ROSA26*<sup>+/Confetti</sup>*Cdh5*<sup>+/ERT2-Cre</sup> animals exposed to TAM at different embryonic stages are also shown (Supplementary Table 4).

Author Manuscript

Author Manuscript

Author Manuscript

Author Manuscript

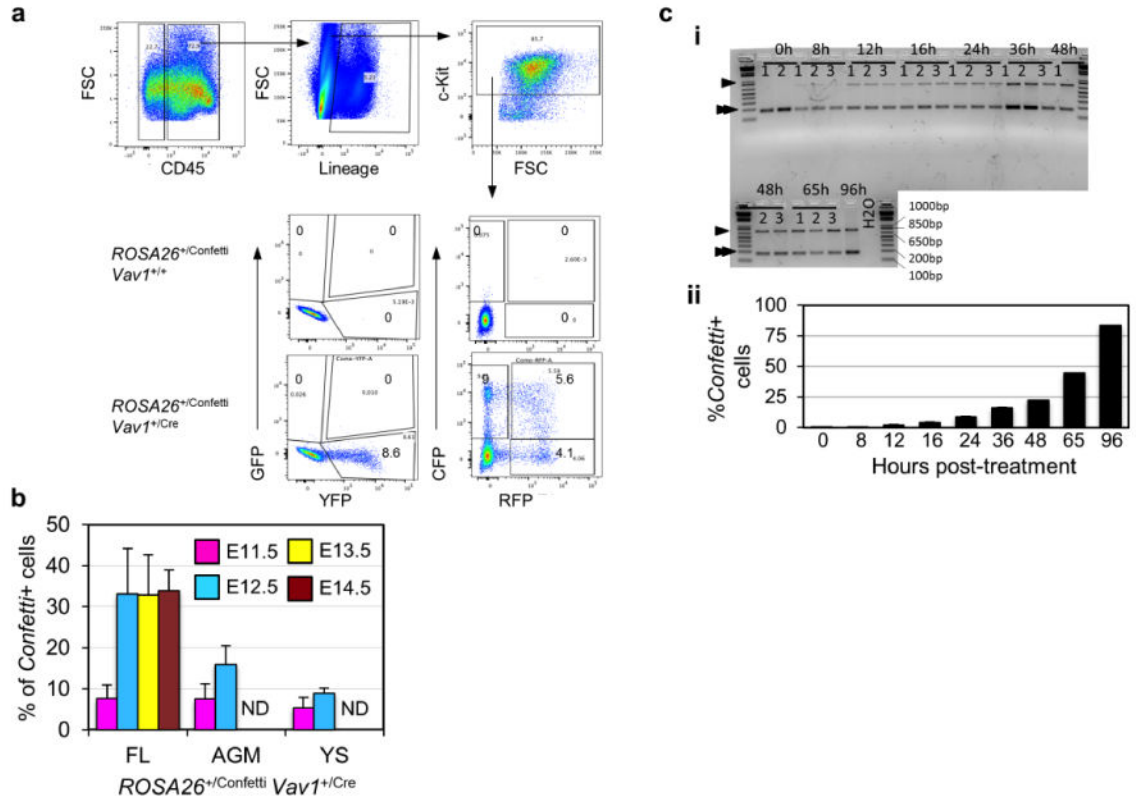


**Figure 4. Onset of *Confetti* labeling in *ROSA26*<sup>+/Confetti</sup> *Vav1*<sup>+/Cre</sup> embryos**

**a**, Representative *Confetti* analysis of CD45<sup>+</sup>Lineage-c-Kit<sup>+</sup> E14.5 *ROSA26*<sup>+/Confetti</sup> *Vav1*<sup>+/Cre</sup> FL cells. RFP+CFP+ cells likely result from residual fluorophore protein previously expressed from same cassette before it “flipped” to allow expression of second fluorophore. **b**, *Confetti* labeling in CD45<sup>+</sup> cells of the FL, AGM, and yolk sac of E11.5 (n=5) and CD45<sup>+</sup>c-Kit<sup>+</sup> cells of E12.5 (n=3), E13.5 (n=13), and E14.5 (n=11) *ROSA26*<sup>+/Confetti</sup> *Vav1*<sup>+/Cre</sup> embryos (Supplementary Table 5). **c**, To assess the temporal delay between allele recombination and detectable fluorescence, iCCs treated with 4-OHT were monitored from 0 to 96 hours post-treatment by genomic PCR (i) and flow cytometry (ii). The average of % of *Confetti*<sup>+</sup> cells is shown (error bars indicate ± s.d. of mean) (n=3) (Supplementary Table 5). Single arrow in (i) indicates recombined *Confetti* allele and double arrow in (i) indicates *Cre* allele as a control for gDNA content. Numbers indicate biological replicates. See Supplementary Fig. 6 for unprocessed scan of the gel.



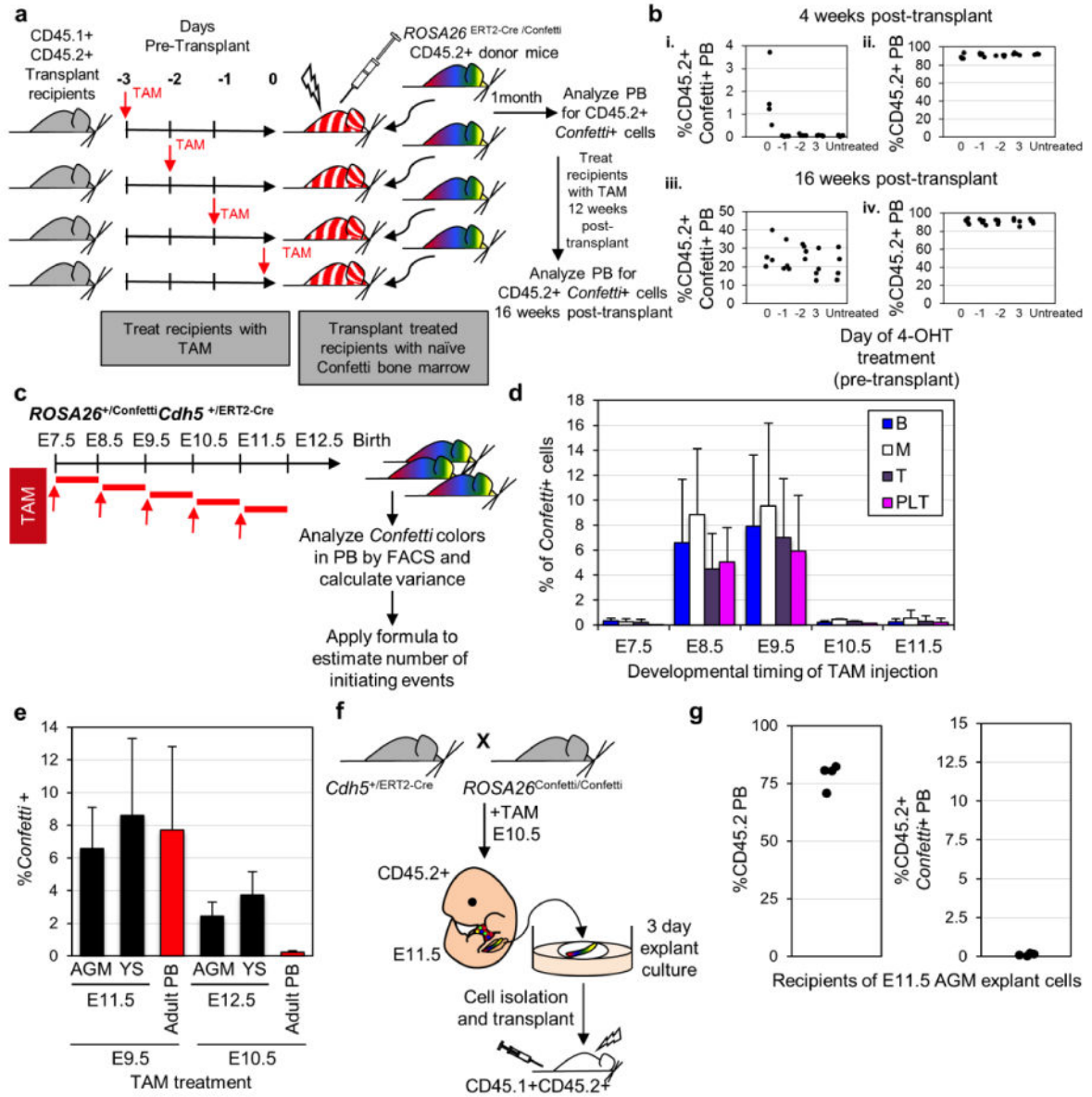


**Figure 5. Hemogenic endothelium is specified between E8.5 and E10.5 of murine ontogeny**  
**a**, Experimental schematic. *ROSA26<sup>ERT2-Cre</sup>/Confetti* (CD45.2+) WBM was transplanted into irradiated CD45.1+CD45.2+ mice treated with a single dose of TAM at 3, 2, 1, or 0 days pre-transplant (n=4 for each time-point). Recipients were treated again with five doses of TAM 12 weeks post-transplant. **b**, i) *Confetti* label in CD45.2+ PB of transplant recipients 4 weeks post-transplant. ii) CD45.2+ PB cells in transplant recipients 4 weeks post-transplant. iii) *Confetti* label in PB of transplant recipients treated again with TAM 12 weeks post-transplant. iv) PB CD45.2+ cells of transplant recipients treated again with TAM 12 weeks post-transplant. **c**, 10 week old *ROSA26<sup>+/</sup>/Confetti<sup>+/</sup>Cdh5<sup>+/</sup>/ERT2-Cre* mice were analyzed for *Confetti* label after exposure to a single dose of TAM at E7.5 (n=6), E8.5 (n=5), E9.5 (n=7), E10.5 (n=5) and E11.5 (n=3, which were 0.03, 0.69, 0.3% *Confetti*+ of total white cells). Two independent litters were analyzed in each cohort. **d**, % *Confetti* label at 10

weeks of age in PB lineages of *ROSA26<sup>+</sup>/Confetti* *Cdh5<sup>+</sup>/ERT2-Cre* mice exposed to TAM during gestation. Error bars indicate  $\pm$  s.d. of mean (Supplementary Table 5). **e**, *Confetti* labeling in VE-Cadherin<sup>+</sup> endothelial cells in the AGM and YS; and in adult PB cells isolated from *ROSA26<sup>+</sup>/Confetti* *Cdh5<sup>+</sup>/ERT2-Cre* mice exposed to TAM during gestation (Supplementary Table 5). **f**, Dams pregnant with CD45.2+ *ROSA26<sup>+</sup>/Confetti* *Cdh5<sup>+</sup>/ERT2-Cre* embryos were treated with a single dose of TAM at E10.5. At E11.5, AGMs were collected (n=4), cultured as explants, and then transplanted. **g**, %CD45.2+ and %CD45.2+ *Confetti*+ PB of recipients of *ROSA26<sup>+</sup>/Confetti* *Cdh5<sup>+</sup>/ERT2-Cre* AGM explant cells four weeks post-transplant (Supplementary Table 5).

Author Manuscript

Author Manuscript

Author Manuscript

Author Manuscript

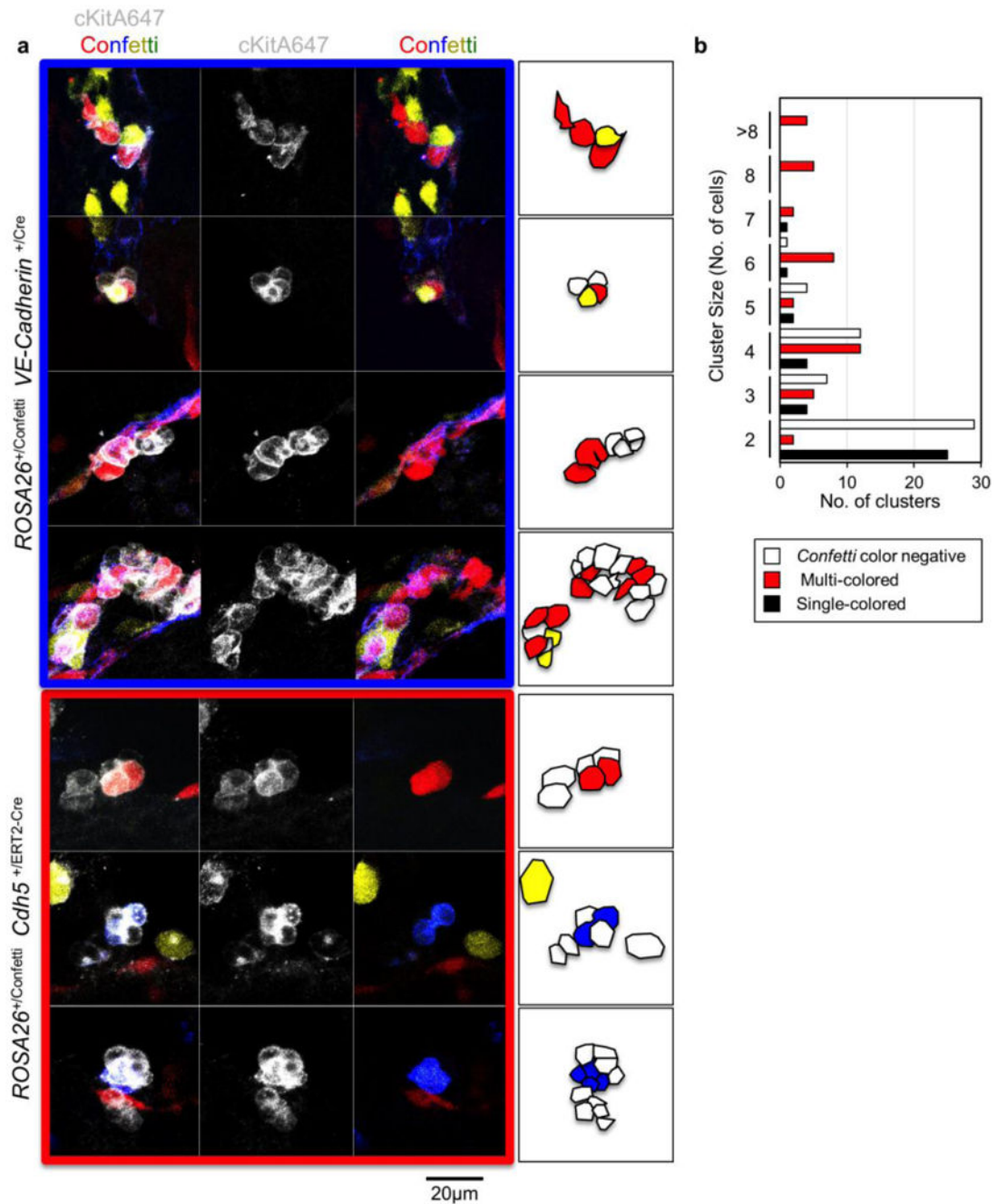


**Figure 6. Intra-aortic cell clusters are polyclonal in origin**

**a**, Analysis of *c-Kit*<sup>+</sup>*Confetti*<sup>+</sup> intra-aortic clusters in E10.5 and E11.5 AGMs isolated from *ROS*A26<sup>+/Confetti</sup> *VE-Cadherin*<sup>+/Cre</sup> embryos or *ROS*A26<sup>+/Confetti</sup> *Cdh5*<sup>+/ERT2-Cre</sup> embryos exposed to TAM at E7.5 and E8.5 of gestation. **b**, E10.5 and E11.5 *ROS*A26<sup>+/Confetti</sup> *VE-Cadherin*<sup>+/Cre</sup> intra-aortic clusters classified by size and cell composition. (2-cell clusters, n=56; 3-cell clusters, n=16; 4-cell clusters, n=28; 5-cell clusters, n=8; 6-cell clusters, n=10; 7-cell clusters, n=3; 8-cell clusters, n=5; 8-cell clusters, n=4) (Supplementary Table 5).

**Estimates of initiating cell numbers**

**Table 1**

	Lineage labeled	TAM treatment	Cell population analyzed for <i>Confetti</i> label	$I_N$	<sup>2</sup> Average Log <sub>10</sub> (CV)	<sup>3</sup> CRE efficiency (%)	<sup>4</sup> Normalized Cell Number Estimate	<sup>5</sup> Confidence Interval
<i>VE-Cadherin<sup>Cre</sup></i>	E11.5 AGM explant; endothelium	-	Blood of transplant recipients	67	7.0334	45	7222	128 – 384
<i>ROSA26<sup>ERT2-Cre</sup></i>	Adult mice; labels all cell types	Adults	Adult blood	7	-1.073	16	8572	5943 – 12,363
<i>E2f<sup>Cre</sup></i>	Pre-implantation; labels all cell types	-	Adult blood	13	0.074	81	828	10 – 81
<i>Flk1<sup>Cre</sup></i>	Multi-potent mesoderm progenitors	-	Adult blood	7	-0.77	66	8719	713– 726
<i>VE-Cadherin<sup>Cre</sup></i>	Endothelium	-	Adult blood	12	-0.626	45	8633	524– 763
<i>Vav1<sup>Cre</sup></i>	HSPCs post-specification		Adult blood	10	-0.75	80	8545	524 - 567
<i>Ubiq<sup>ERT2-Cre</sup></i>	Ubiquitous	E7.5	Adult blood	5	-0.26	12	9617	324-1174
<i>Ubiq<sup>ERT2-Cre</sup></i>	Ubiquitous	E8.5	Adult blood	6	-0.23	13	9538	273-1057
<i>Cdh15<sup>ERT2-Cre</sup></i>	Endothelium	E8.5	Adult blood	5	-0.172	16	9341	161 – 723
<i>Cdh15<sup>ERT2-Cre</sup></i>	Endothelium	E9.5	Adult blood	7	-0.152	16	9319	147 – 691

<sup>1</sup> Number of mice, embryos, or transplant recipients

<sup>2</sup> GFP is excluded from all analyses, because GFP+ PB cells always fell below the minimum threshold for precision

<sup>3</sup> CRE efficiency calculated as % labeling of the total PB

<sup>4</sup> Estimates normalized to CRE efficiency =  $(10^{(-1.56 * \text{Log}_{10}(\text{CV}) + 1.47)})^{(\text{efficiency}/100)}$

<sup>5</sup> 95% confidence interval calculated as:  $(10^{(-2.1 * \text{Log}_{10}(\text{CV}) + 1.06)}) - (10^{(-1.02 * (\text{Log}_{10}(\text{CV}) + 1.89))})$

<sup>6</sup> Seven independent explants transplanted into seven recipients

<sup>7</sup> 16 weeks post-transplant

<sup>8</sup> Based on analysis of mice between 10 and 16 weeks of age of both sexes

<sup>9</sup> Based on analysis of mice at 10 weeks of age of both sexes

Please see also Supplementary Table 4